Journal of Applied Fluid Mechanics, Vol. 18, No. 8, pp. 2095-2107, 2025.
Available online at www.jafmonline.net, ISSN 1735-3572, EISSN 1735-3645.
https://doi.org/10.47176/jafm.18.8.3310

Optimization of Structural Parameters and Cavitation Suppression in Control Valves Based on P-WOA

W. Li, S. Li†, J. Hou, L. Yang and Y. Tian

School of Petrochemical Engineering, Lanzhou University of Technology, Lanzhou 730050, PR China
Machinery Industry Pump Special Valve Engineering Research Center, Lanzhou 730050, PR China

†*Corresponding Author Email: Li192024@163.com*

ABSTRACT

A control valve is a critical component in water supply systems, controlling pressure, flow, and direction. However, cavitation, caused by low pressure in the valve cavity, disrupts flow and leads to cavitation damage, vibration, and noise, affecting valve reliability and system stability. In this study an optimization method for controlling valve structural parameters is proposed to reduce cavitation-induced flow resistance and enhance flow capacity. Using the orifice throttling principle, the continuity equation, and Bernoulli's equation, the relationship between cavitation-induced resistance and flow rate is analyzed. Numerical calculations reveal that cavitation is most severe at a 40% valve opening, which is further studied. Boosting method integrates reinforcement learning PPO with the whale optimization algorithm (WOA) to form the P-WOA model. SOLIDWORKS and CFD software are used for parametric modeling, and a control valve structural parameter database is created using Latin hypercube sampling. The database is input into the P-WOA model for training to find optimal valve parameters. These solutions are then globally optimized by the WOA. The simulation and experimental results show that the P-WOA-optimized valve parameters significantly reduce cavitation (the gas volume fraction is reduced by 99.8% compared with the original and 59.6% compared with the PPO optimization) and improve the flow capacity. This proves the effectiveness of the P-WOA model and provides a new structural optimization solution for reducing cavitation in engineering.

Article History

Received December 15, 2024
Revised March 8, 2025
Accepted March 10, 2025
Available online June 3, 2025

Keywords:

Control valve
Throttling orifice
Cavitation flow
Reinforcement learning
Whale optimization algorithm

1. INTRODUCTION

Valve-controlled piping systems play important roles in regulating, controlling and maintaining the safety of the overall system, and are widely used in the fields of construction, shipbuilding, petroleum, fire protection engineering, aerospace, etc. (Hou et al., 2021; Rabelo et al., 2023; Ou et al., 2024; Park et al., 2024). Especially in the water supply system of buildings, control valves are used to control the water flow pressure, ensure the water pressure balance between different floors, and avoid the problem of insufficient water supply on high floors or excessive water pressure on low floors (Han et al., 2020; Xie et al., 2020; Chen et al., 2023). However, cavitation may occur in the actual operation of the control valve, which has an adverse effect on the safety and operation efficiency of the system. The bursting of bubbles in the cavitation phenomenon will produce high-energy impact, which directly acts on the internal components of the control valve, especially the valve core and valve seat, causing erosion and wear of the material, thereby reducing the sealing performance of the control valve (Hou et al., 2021; Zhang et al., 2024). Long-term cavitation impact may cause the control valve to fail, thereby affecting the stability and useful life of the water supply system.

Under a normal-temperature working environment, when the local pressure of the liquid is lower than the saturated vapor pressure, the original "gas core" or tiny bubbles in the liquid will gradually grow into visible bubbles and collapse at high pressure. This process is called cavitation phenomenon (Guo et al., 2023; Jia et al., 2024). This phenomenon is more likely to occur in pure water pressure system components, especially in angle control valves. During use, angle control valves will face a series of inherent problems such as vibration and noise (Wang et al., 2024a). In particular, under high pressure and large flow conditions, cavitation of varying degrees will occur. Regardless of the cavitation flow state, the actual flow area and flow coefficient of the control valve flow channel will change, thereby causing unstable vibration of the control valve (Fu et al., 2023). Therefore, some scholars have tried to reduce the cavitation effect of the control valve by optimizing the structure of the control valve. For example, Han et al. (2020) selected three typical cone valve structures and conducted numerical research on the flow and cavitation characteristics of water pressure cone valves. The experimental results show that the designed two-stage throttle valve (TS valve) effectively suppresses cavitation. Wang et al. (2024b) verified the relationships among the cavitation area, flow velocity and sound pressure level through simulations and experimental comparisons. Li et al. (2022) used CFD to analyze the internal flow field of a centrifugal pump and obtained the optimal combination of blade wrapping angle and blade installation angle, further improving the anti-cavitation ability of the centrifugal pump.

Most of the above methods are based on the experience of researchers in designing calculations. Although they have achieved good results, they are inefficient and not suitable for the current industry development trend. With the continuous improvement of computer capabilities, effective optimization algorithms such as machine learning and reinforcement learning have been continuously proposed (Ergur, 2022; Shijo & Behera 2023; Deng et al., 2024; Mashhadi et al., 2024; Naik & Naik 2024; Xia et al., 2024). An increasing number of researchers are attempting to combine optimization algorithms with simulation software such as CFD to make full use of the powerful computing power of computers to further improve computing efficiency. For instance, Trilling et al. (2024) used reinforcement learning (RL) to optimize the vehicle frame model and the vehicle rocker arm model with enhanced Graph and Heuristic-based Topology optimization (GHT), and evaluated the optimization performance of the model in a real environment. Hu et al. (2022) proposed a method that combines multi-objective optimization and deep reinforcement learning to solve the problem of water valves and fire hydrants isolating contaminated water. The simulation results show that this method can effectively isolate contamination and reduce risks to customers. Xin et al. (2024) developed a new reinforcement learning algorithm that effectively improved the control efficiency and reliability of smart valves in heating systems. Homod et al. (2023) proposed a deep clustering model based on deep clustering of lagrangian trajectories for multi-task learning (DCLTML) to optimize building structures and achieve the purpose of reducing building energy consumption. Experimental results show that this method can minimize energy consumption compared with traditional methods. Although the above methods have achieved good optimization results in different fields, in practical applications, reinforcement learning consumes large computing resources (Zhu et al., 2023) and is prone to falling into local optimal solutions (Akers & Barton 2024). These problems become more prominent when dealing with complex multi-objective optimization.

The effective proposal of the whale optimization algorithm (WOA) provides an optimization approach for the above problems. The training of reinforcement learning requires a lot of time and data, while the results of WOA can be used as initial values to provide the reinforcement learning model, thereby greatly shortening the convergence time of the reinforcement learning model and improving the optimization efficiency. Wadood et al. (2024) proposed a hierarchical WOA to optimize the wind power and thermal power hybrid system. The effectiveness of the proposed method was verified by statistical analysis of the minimum fitness value. Zeng et al. (2021) proposed an improved whale algorithm to optimize the structural size of the turbine disc section. The experimental results show that the improved WOA converges faster and is more practical in practical engineering problems. Ding et al. (2024) used the WOA combined with support vector regression to optimize the valve closing parameters involved in the booster pump station. The study shows that the proposed method effectively solves the multi-objective optimization problem of water hammer protection in the system. Although the WOA algorithm has certain advantages, it still has some disadvantages. For example, WOA has a strong global search capability, but in the later stage of iteration, its convergence speed is often slow, especially when facing fine tuning tasks, the optimization efficiency is low. Therefore, it still needs to be optimized in practical problems.

In summary, the cavitation problem faced by the control valve in the water pressure system. This study proposes a parameter optimization model based on the joint drive of PPO and WOA. This method first uses CFD and SOLIDWORKS software to achieve joint parametric modeling, and subsequently establishes a sample database through Latin hypercube sampling. Then, the database is learned using joint-driven reinforcement learning and WOA algorithms. Because the training of PPO requires a lot of time and data, the results of WOA can be provided to PPO as initial values, thereby greatly shortening the convergence time of PPO and improving the efficiency of optimization. Finally, the WOA is used again to optimize the structural parameters and predicted values to improve the reliability of the prediction results.

2. PRELIMINARIES

2.1 Model of Turbulence

The commonly used turbulence models in CFD software mainly include $k-\varepsilon$, $k-\omega$ and large eddy simulation (LES) (Liu et al., 2024). Many researchers (Yanez & Class 2022; Liu et al., 2023; Mohsenabadi et al., 2023) have shown that the $k-\varepsilon$ model has certain advantages in calculating the onset of cavitation. Therefore, the standard $k-\varepsilon$ model is selected for subsequent turbulence calculations in this study. The specific calculation is as follows:

$$\frac{\partial}{\partial t}(\rho k)+\frac{\partial}{\partial x_i}(\rho k u_i)=\frac{\partial}{\partial x_j}\left[(\mu+\frac{\mu_t}{\sigma_k})\frac{\partial k}{\partial x_j}\right]+G_k+G_b-\rho\varepsilon-Y_M+S_k \tag{1}$$

$$\frac{\partial}{\partial t}(\rho\varepsilon)+\frac{\partial}{\partial x_i}(\rho\varepsilon u_i)=\frac{\partial}{\partial x_j}\left[(\mu+\frac{\mu_t}{\sigma_\varepsilon})\frac{\partial\varepsilon}{\partial x_j}\right]+C_{1\varepsilon}\frac{\varepsilon}{k}(G_k+C_{3\varepsilon}G_b)-C_{2\varepsilon}\rho\frac{\varepsilon^2}{k}+S_\varepsilon \tag{2}$$

where σ_k is the turbulent Prandtl number of turbulent kinetic energy; G_k is the generation term of turbulent kinetic energy k caused by the average velocity gradient; G_b is the generation term of turbulent kinetic energy k caused by buoyancy; σ_ε is the turbulent Prandtl number of turbulent dissipation rate; Y_M is the fluctuation of the total dissipation rate caused by pulsating expansion in compressible turbulence; $C_{1\varepsilon}$, $C_{2\varepsilon}$ and $C_{3\varepsilon}$ are empirical constants; S_k and S_ε are source terms defined by the user according to the calculation conditions.

2.2 Model of Cavitation

In the numerical simulation part of this study, the Schnerr-Sauer (Li et al., 2020; Ruetten et al., 2023; Wang et al., 2023; Zhang et al., 2023) model is used as the cavitation model. The specific calculation of the vapor phase volume fraction in this model is as follows:

$$\frac{\partial}{\partial t}(\alpha\rho_v)+\nabla\cdot(\alpha\rho_v\vec{V})=\frac{\rho_v\rho_v}{\rho}\frac{D\alpha}{Dt} \tag{3}$$

The phase change transmissibility is:

$$R_x=\frac{\rho_v\rho_l}{\rho}\frac{d\alpha}{dt} \tag{4}$$

The gas phase volume fraction is:

$$\alpha=\frac{n_b\frac{4}{3}\pi R_B^3}{1+n_b\frac{4}{3}\pi R_B^3} \tag{5}$$

where R_x is the mass transfer efficiency; R_B is the bubble radius (He et al., 2023).

$$R_x=\frac{\rho_v\rho_l}{\rho}\alpha(1-\alpha)\frac{3}{R_B}\sqrt{\frac{2}{3}\frac{(p_v-p)}{\rho_l}} \tag{6}$$

$$R_B=(\frac{\alpha}{1-\alpha}\frac{3}{4\pi}\frac{1}{n})^{\frac{1}{3}} \tag{7}$$

Finally, the phase change rate of the model is as follows:

$$R_e=\frac{\rho_l\rho_v}{\rho}\alpha(1-\alpha)\frac{3}{R_B}(\frac{2}{3}\frac{p_v-p}{\rho_l})^{\frac{1}{2}} \quad ; p\le p_v \tag{8}$$

$$R_c=\frac{\rho_l\rho_v}{\rho}\alpha(1-\alpha)\frac{3}{R_B}(\frac{2}{3}\frac{p-p_v}{\rho_l})^{\frac{1}{2}} \quad ; p\ge p_v \tag{9}$$

where R_e is the steam generation rate; R_c is the steam condensation rate.

Figure 1 shows the pressure and velocity curves of the fluid flowing through the control valve port, as well as the cavitation phenomenon behind the throttle hole.

Figure 1a shows that when the fluid passes through the throttling orifice, the flow rate increases, causing the local pressure at that location to decrease. When the local pressure p_{vc} at that location is equal to or less than the saturated vapor pressure p_v of the gas under the same working conditions, cavitation occurs. From Figure 1b, it can be observed that because of the cavitation phenomenon after the throttling orifice, many cavitation bubbles gather here. The presence of these bubbles hinders the flow of the fluid medium, forming a blocked flow. On the other hand, when the fluid flows through the throttling orifice, the flow rate is decrease, the fluid pressure rises, and the cavitation bubbles are compressed and deformed. When the deformed cavitation bubbles reach a critical size, they will rupture, thereby generating noise.

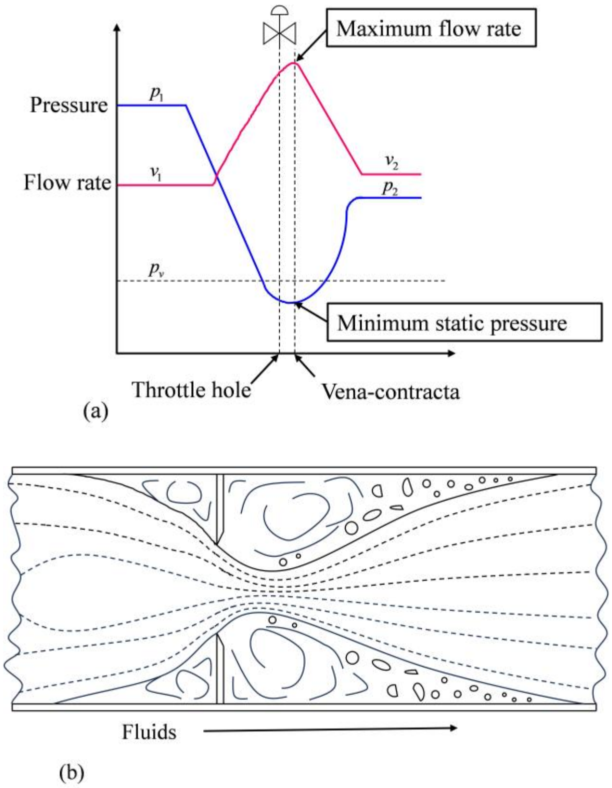

Fig. 1 Control valve cavitation phenomenon. (a) Pressure and velocity change curves when fluid flows through the control valve. (b) Cavitation phenomenon behind the throttle orifice

2.3 Reinforcement Learning (RL)

Reinforcement learning is a machine learning framework in which intelligent agents interact with the environment and continuously try and fail, receive rewards and adjust strategies in order to maximize long-term benefits in a complex environment (Park et al., 2023; Yin et al., 2024). Among them, proximal policy optimization (PPO) was proposed by Schulman et al. (2017) as an intelligent algorithm in RL. The PPO algorithm mainly approximates the policy function and the value function through two neural networks: the Actor network outputs the mean and standard deviation of the current state, and sampling it can obtain the next step $a_t \sim N(\mu_\vartheta,\upsilon_\vartheta^2)$, where ϑ is the network parameter of the Actor; the Critic network outputs the value $V_\phi(s_t)$ of the current state, where ϕ is the network parameter of the Critic. PPO optimizes the strategy mainly by relying on the advantage function A^π. The specific calculation is as follows:

$$A^\pi(s,a)=Q^\pi(s,a)-V^\pi(s) \tag{10}$$

For further calculations, PPO usually replaces A^π with the advantage estimate $\hat{A}^\pi$, which is expressed as follows:

$$\hat{A}_j^\pi=\sum_{l=j}^{|D|-1}(\gamma\lambda_{GAE})^{l-j}K_l \tag{11}$$

$$K_l=R_l+\gamma V_\phi(s_{l+1})-V_\phi(s_l) \tag{12}$$

where $|D|$ is the data set; $\lambda_{GAE}\in[0,1]$ is the GAE discount factor; K_l is the time series difference error.

The PPO algorithm inherits the stability and reliability of the trust region policy optimization (TRPO) algorithm and further reduces the difficulty of calculation, thus improving the overall performance of the algorithm. The parameter updates of the actor and critic networks are as follows:

$$w_{t+1} = w_t + \alpha^w \delta_t \nabla V(s_t, w_t) \quad (13)$$

$$\delta_t = R_t + \gamma V(s_{t+1}, w_{t+1}) - V(s_t, w_t) \quad (14)$$

$$\theta_{t+1} = \theta_t + \alpha^\theta \delta_t \nabla \lg \pi_{\theta_t}(a_t \mid s_t) \quad (15)$$

where w_t and θ_t are the parameters of the Actor and Critic networks at time t; α^w and α^θ are the update steps of the two network parameters respectively; δ_t is the temporal difference error value, indicating the direction and size of the parameter update; R_t is the environmental reward at time *t*.

2.4 Whale Optimization Algorithm (WOA)

The WOA is a new swarm intelligence optimization algorithm proposed by Mirjalili & Lewis (2016) in 2016. It simulates the hunting behavior of humpback whales using bubble nets and can achieve the goal of finding the optimal target in a global range (Nadimi-Shahraki et al., 2023). According to the predation behavior of whales, it can be divided into three stages: encirclement predation, bubble net predation, and random search for prey (Dadashzadeh et al., 2022). Assuming that the number of whales in the population is *N* and the dimension is *D*, the position of each whale in the algorithm represents a feasible solution. During the predation process, the position of the *i*-th whale in the *D*-dimensional space is $A_i(a_i^1, a_i^2, \cdots, a_i^D)$, $i = 1, 2, \cdots, N$, where the optimal whale position, that is, the position of the prey, corresponds to the global optimal solution.

In the process of encircling and hunting, whales can change their own position according to the location of their prey. In the process of algorithm optimization, it is assumed that the optimal solution of the evaluation function of the control valve structure parameter switching is the location of the target prey. The specific calculation is as follows:

$$\vec{D} = \left|\vec{C} \cdot \vec{A}^*(t) - \vec{A}(t)\right| \quad (16)$$

$$\vec{C} = 2 \cdot \vec{r} \quad (17)$$

where t is the current iteration number; $\vec{A}^*(t)$ is the optimal position in the *t*-th generation of whales; $\vec{A}(t)$ is the position of the *t*-th generation of whales; $\vec{C}$ is the swing factor.

The position update formula of individual whales is:

$$\vec{A}(t+1) = \vec{A}^*(t) - \vec{M} \cdot \vec{D} \quad (18)$$

$$\vec{M} = 2\vec{m} \cdot \vec{r} - \vec{m} \quad (19)$$

where $\vec{M}$ is the convergence factor; $\vec{r}$ is a random number between [0,1]; $\vec{m}$ decreases linearly from 2 to 0 as the number of iterations increases.

3. Proposed Method and Research Subjects

In the second section, the relevant theoretical knowledge of turbulence model, cavitation model, reinforcement learning and whale optimization algorithm involved in this study is introduced. This section further explores the control valve structural parameter optimization model constructed in this study.

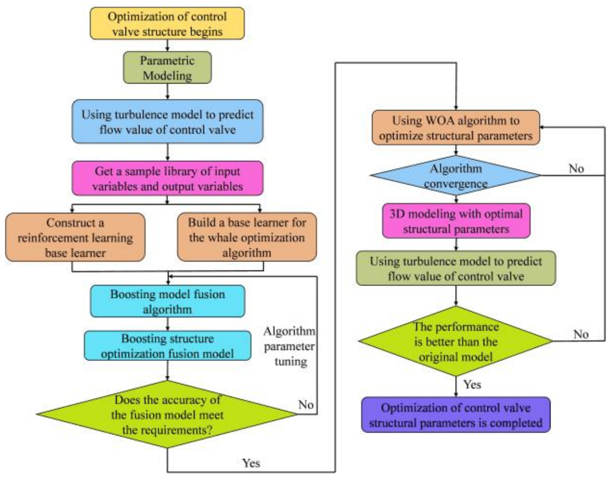

Fig. 2 Architecture of the P-WOA model

3.1 The Proposed P-WOA Model

Figure 2 shows the proposed control valve structural parameter optimization flow chart. The figure, clearly shows the specific steps of control valve optimization. At the beginning of structural optimization, we first use Latin hypercube sampling to sample the parameters to be optimized, and establish a database containing 100 sets of data through the joint parameter drive of CFD software and SOLIDWORKS software. Subsequently, the Boosting method is used to effectively integrate the PPO model and the WOA algorithm to train and learn the established database. Finally, the structural parameters that meet the conditions are re-entered into the WOA algorithm for optimization, and the optimal results are applied to create the three-dimensional model to obtain the optimized control valve.

To further explain the implementation steps of the P-WOA optimization model, the specific calculation is shown in Algorithm 1:

Algorithm 1 P-WOA model framework

Input: $X(a_1, a_2, a_3, \cdots, a_n)$

Output: $Y(a_1', a_2', a_3', \cdots, a_n')$

for $i \in \{1, \cdots, N\}$ **do**

Run policy π_θ for T timesteps, collecting $\{s_t, a_t, r_t\}$

Estimate advantages $\hat{A}_t = \sum_{t'>t} \gamma^{t'-t} r_{t'} - V_\phi(s_t)$

$\pi_{old} \leftarrow \pi_\theta$

for $j \in \{1, \cdots, M\}$ **do**

$$J_{PPO}(\theta) = \sum_{t=1}^{T} \frac{\pi_\theta(a_t \mid s_t)}{\pi_{old}(a_t \mid s_t)} \hat{A}_t - \lambda \mathrm{KL}\left[\pi_{old} \mid \pi_\theta\right]$$

Update θ by a gradient method w.r.t. $J_{PPO}(\theta)$

Introducing the WOA algorithm

Calculate the fitness of each search agent

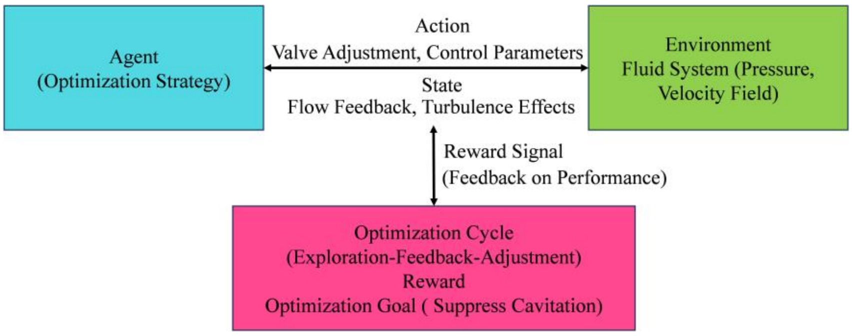

Fig. 3 Reinforcement learning optimization framework

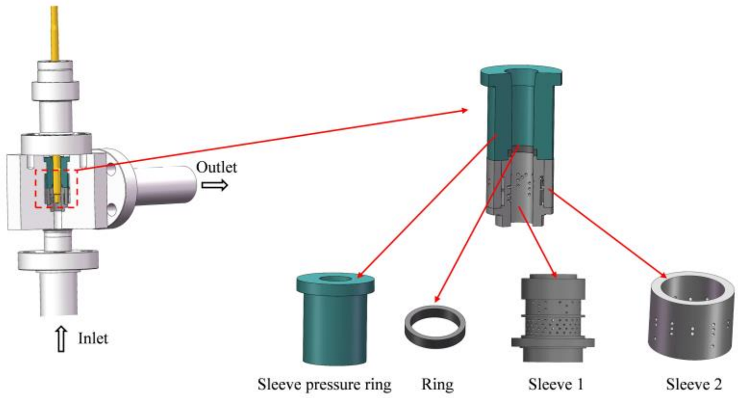

Fig. 4 Schematic diagram of the control valve structure

X^* = the best search agent

while (t < maximum number of iterations)

for each search agent

Update a, A, C, l, and p

if ($p < 0.5$)

if ($|A| < 1$)

Update the position of the current search agent by the Eq. (16)

Introduce physical boundary conditions

if $\mathrm{KL}[\pi_{old} | \pi_\theta] > \beta_{high}\mathrm{KL}_{target}$ **then**

$\lambda \leftarrow \lambda\alpha$

Introduce physical boundary conditions

else if $\mathrm{KL}[\pi_{old} | \pi_\theta] < \beta_{low}\mathrm{KL}_{target}$ **then**

$\lambda \leftarrow \lambda / \alpha$

else if $\beta_{low}\mathrm{KL}_{target} < \mathrm{KL}[\pi_{old} | \pi_\theta] < \beta_{high}\mathrm{KL}_{target}$

$\lambda \leftarrow \mathrm{maintain}(\lambda)$

Use WOA algorithm again for global optimization

end

return the best vector Y

Figure 3 shows the application framework of the reinforcement learning algorithm in fluid mechanics optimization. The figure is divided into three main parts: agent, environment (fluid system) and optimization cycle. The agent represents the optimization strategy and is responsible for adjusting the valve structure parameters in the fluid system to achieve the optimization goal (suppressing cavitation). The environment is the fluid system itself, which contains physical properties such as pressure and velocity fields. The agent interacts with it and drives the optimization process by changing the fluid state. The optimization cycle includes the steps of exploration, feedback and adjustment. The agent adjusts according to the environmental feedback and continuously optimizes until the expected goal is achieved. In addition, the reward mechanism feedbacks the effect of the agent's behavior and evaluates whether the optimization is successful.

3.2 Study Subjects

The computing resources used in this experiment are: SOLIDWORKS 2021, Inter(R) Core (TM) i9-14900HX, NVIDIA GeForce RTX 4060, and the code running platform is JUPYTER NOTEBOOK and ANSYS Workbench 2020 R2. In the numerical calculation process, the computational fluid dynamics (CFD) software ANSYS CFX is used, and the CFX solver adopts the finite volume method (FVM) (Li et al., 2025).

Figure 4 shows the basic structure of the control valve used in this study. According to the figure, the control valve is mainly composed of components such as a valve body, a valve stem, a sleeve pressure ring, a sleeve and a sealing ring.

Figure 5 shows the overall pipeline and environmental facilities of the relevant experiments, which include components such as the control valve, flow

Fig. 5 Control valve flow characteristics testing system

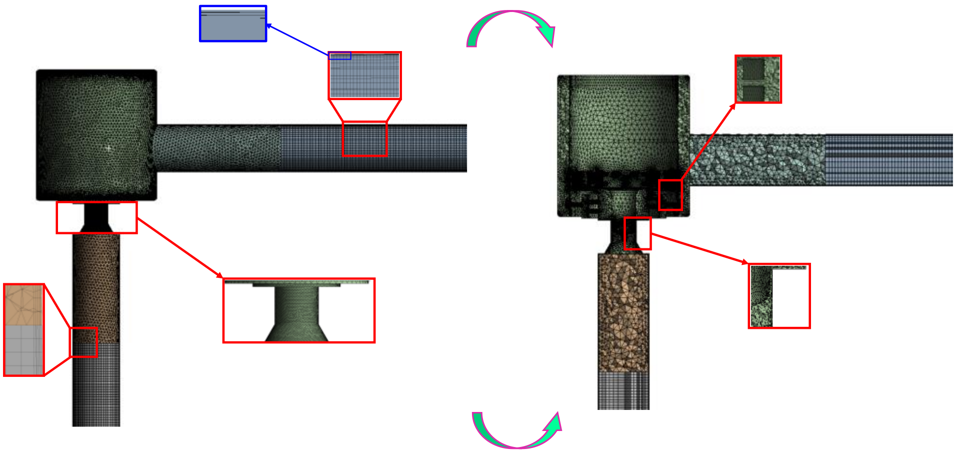

Fig. 6 Control valve flow channel mesh division

measurement instrument, pressure measurement instrument and controller. In this experiment, the experimental medium is water. The medium is at one atmosphere, the temperature is 25 ℃, the density is 997 kg/m3, and the dynamic viscosity is 8.8987e-04 Pa·s.

3.3 Calculation Settings and Grid Independence Verification

Since the flow field inside the control valve is a complex multiphase flow and there is a transition from liquid to steam in the cavitation region (Ou et al., 2015), in the numerical calculation process, in order to make the results closer to the experimental results, the relative slip velocity between the bubble and the liquid phase and gravity is ignored, and the mixed-phase model, standard $k-\varepsilon$ turbulence model and Schnerr-Sauer model are used to describe the flow phenomenon of the medium in the control valve. Among them, the relative slip velocity is ignored, mainly because the slip velocity between the bubble and the liquid phase is small compared with the overall flow, so this factor can be ignored.

We use meshing preprocessing software to mesh the three-dimensional model of the control valve, and combine it with CFD software for numerical simulation. Owing to the narrow and long opening of the control valve, the gradient of pressure and velocity changes significantly, and the flow field characteristics at the valve opening are relatively complex. Therefore, it is necessary to locally refine the grid in the valve opening area to ensure the convergence of the calculation and the reliability of the results. Moreover, we make full use of the advantages of tetrahedral and hexahedral meshes to divide the flow channel of the control valve into a mixture of tetrahedral and hexahedral meshes. Figure 6 shows the division result of the control valve flow channel. In the figure, we have marked the valve port, the throttle orifice, the tetrahedral mesh part and the hexahedral mesh part. In the grid settings, the y+ value is 32, the thickness of the first grid layer is 0.5, 5 boundary layers are set in the valve body, the growth rate is 1.2, and the Reynolds number is 62144.98.

Figure 7 shows the mass flow rates corresponding to different numbers of grids when the control valve is fully open. To improve the calculation efficiency and ensure the accuracy of the results, we set five schemes and present their corresponding flow values in the figure. The analysis results show that starting from cell-3, no matter how the number of grids changes, the change in mass flow rate is small. Compared with cell-3, the mass flow rate differences between cell-4 and cell-5 are within 5%. Therefore, in order to optimize the calculation efficiency, we choose cell-3 (the number of grid nodes and units are

Table 1 Parameter variable constraint range

Design variables	Initial value	Lower critical value	Upper critical value
Orifice diameter a_1 (mm)	1.5	1	3
Orifice spacing a_2 (mm)	0.5	0.1	1
Sleeve spacing a_3 (mm)	2.5	2.5	4
Orifice arrangement angle a_4 (°)	15	15	60

Table 2 Part of the database sampling results

Serial number	Orifice diameter a_1 (mm)	Orifice spacing a_2 (mm)	Sleeve spacing a_3 (mm)	Orifice arrangement angle a_4 (°)
1	2.482590	0.246860	2.883160	20
2	1.894959	0.913157	3.760215	15
3	2.244349	0.555909	2.727291	50
		…	…	
98	1.692414	0.112436	3.586812	5
99	2.769254	0.701233	3.019198	45
100	1.331492	0.662906	2.668320	10

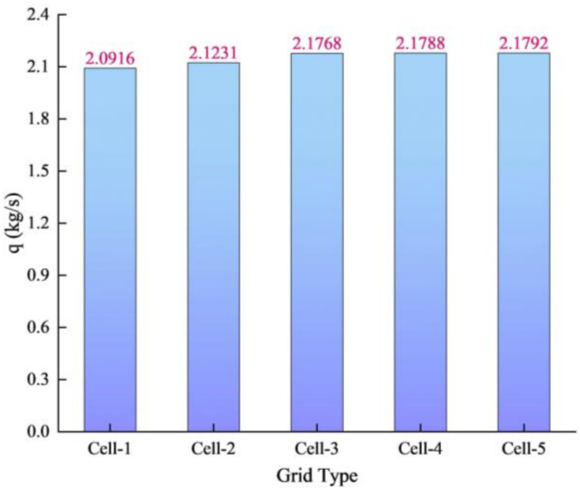

Fig. 7 Mass flow rate at different mesh sizes

328,476 and 1,130,274 respectively) for further calculation. When conducting grid independence studies, we used the ratio of the outlet static pressure P_{out} to the inlet total pressure P_{in} (P_{out}/P_{in}) of 0.8392. These boundary conditions were chosen mainly to reflect the working state of the control valve under actual operating conditions.

Moreover, to further demonstrate the necessity of optimizing the control valve structural parameters, the next study will analyze the control valve at 40% opening. The total stroke of the control valve is 23mm, so at 40% opening, the valve core will move upward 9.2mm from the fully closed state.

4. RESULTS AND ANALYSIS

4.1 Control Valve Structure Optimization and Parameter Setting

Before building the proxy model for optimizing the structural parameters of the angle control valve, we measured the mass flow rate of the non-optimized control valve on the test bench to be 0.676 kg/s, while the numerical calculation result was 0.644 kg/s. In contrast,

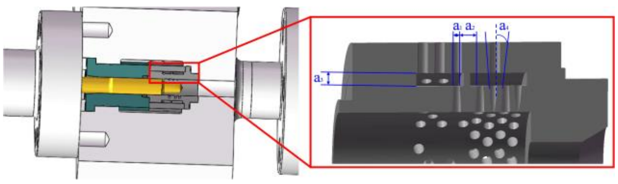

Fig. 8 Parametric modeling of multistage sleeve

the mass flow rate of the initially designed control valve was 0.77 kg/s, which failed to reach the expected flow rate and there was a significant gap, which may be due to the additional flow resistance caused by cavitation. Next, we will analyze the classic opening of the control valve of 40%, perform parametric linkage through SOLIDWORKS and CFD software, and perform multiple simulation analyses on the multi-stage pressure drop sleeve of the control valve.

To explore the influence of the four parameters of the throttle hole diameter a_1, hole spacing a_2, sleeve spacing a_3 and hole arrangement angle a_4 of the inner sleeve of the control valve on the flow characteristics and cavitation phenomenon of the angular control valve, Fig. 8 shows the specific parameter annotations after parametric modeling of the inner sleeve of the control valve.

In addition, to further constrain the prediction accuracy of the subsequent proxy model, Table 1 shows the constraint range of the four parameter variables to further improve the accuracy and authenticity of the database.

The reliability of the constructed prediction model depends on the model's ability to learn from the database, so the construction of a good database is crucial. Based on Table 1, the optimal Latin hypercube sampling method is used to construct the database in the spatial range. To ensure the uniformity of the data sample and reduce the prediction blind area, 100 sampling points are set, which can ensure that the actual scene changes are fully covered while avoiding overfitting or bias. Table 2 shows some sampling results of the database.

Table 3 Structural parameters of sleeve before and after optimization

Design variables	Before optimization	PPO model results	P-WOA model results
Orifice diameter a_1 (mm)	1.5	2	2.5
Orifice spacing a_2 (mm)	0.5	0.3	0.5
Sleeve spacing a_3 (mm)	2.5	2.8	3
Orifice arrangement angle a_4 (°)	15	20	60
Hole number	56	74	38

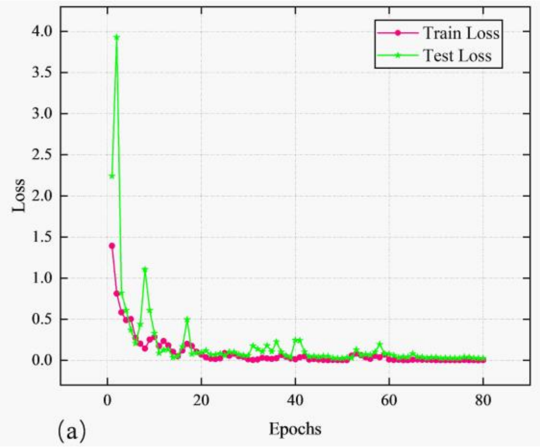

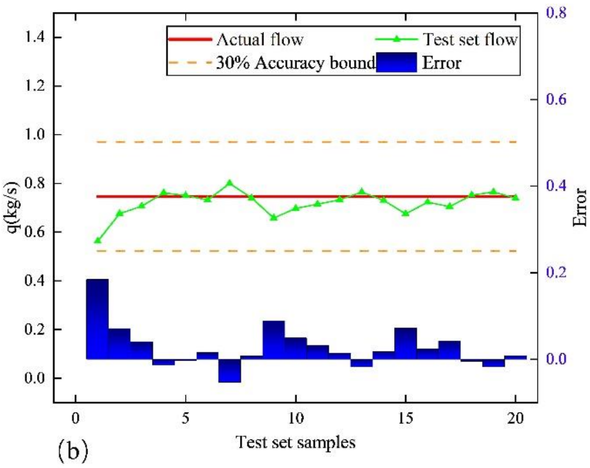

Fig. 9 Loss and test set results. (a) Training set and test set loss curves. (b) Test set verification results

4.2 Model Training and Result Analysis

The data in Section 4.1 are input into the P-WOA model we built for model training and parameter optimization. The entire training process is carried out on the JUPYTER NOTEBOOK platform. The optimizer is Adam, and the dataset is divided into 8:2 ratios, with 80% for training and 20% for testing. Figure 9 shows the loss curves of the training set and test set during the training process, as well as the verification results of the test set.

Figure 9a shows the training loss and test loss of the constructed model during the training process. The results show that both curves show good convergence. Figure 9b shows the similarity between the 20% test set flow value and the actual flow value. The prediction results are all within the accuracy range of 30%, which verifies the reliability of the model. The figure, reveals that the test set results are generally stable and very close to the experimental values. The blue bar graph in the figure represents the error between the predicted value and the actual value. Although the error of individual values is large, the overall trend is relatively stable. Therefore, Fig. 9 further proves the superiority and reliability of our proposed model.

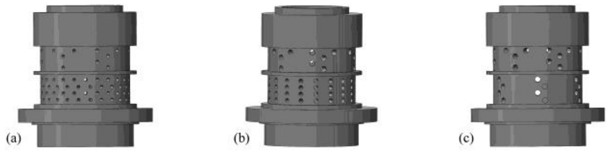

Fig. 10 Results before and after sleeve optimization. (a) Structure before optimization. (b) PPO optimization results. (c) P-WOA optimization results

Based on the above results, the optimal result of the P-WOA model is shown in Fig. 9. To further highlight the superiority of our proposed model, the results of the single PPO model are also listed in Fig. 10 for comparison.

As shown in the figure, the results after P-WOA model optimization are significantly different from those before optimization and those after single PPO optimization in different structural parameters, especially in terms of the number and arrangement of holes.

Table 3 shows the specific structural parameters before optimization, the single PPO optimization results, and the optimized P-WOA model we propose.

4.3 Effects of Sleeve Structure on the Flow Force and Cavitation Characteristics

In the numerical simulation of this section, the change law of water flow force and cavitation characteristics before and after the sleeve optimization in Section 4.2 is discussed. By comparing the PPO results with the results of the proposed P-WOA model, the accuracy and reliability of the proposed method are further emphasized. The pressure distribution cloud map before optimization and the two optimization results is shown in Fig. 10. It can be seen from the Fig. 11 that the flow channel inlet is a high-pressure distribution area, while the downstream flow channel is a low-pressure distribution area, and the pressure drop is mainly concentrated at the throttling orifice. Compared with the results before optimization, the pressure distribution in Fig. 11b is more uniform; and. 11c shows that compared with Figs 11a and 11b, the pressure distribution at the throttling orifice is also more uniform, and is not concentrated in a specific position. This is mainly attributed to the change in the internal structure of the flow channel, which causes the flow direction of the high-speed fluid to deviate, forming a high-speed vortex, and the central area is often accompanied by a vacuum effect, thereby further reducing the pressure.

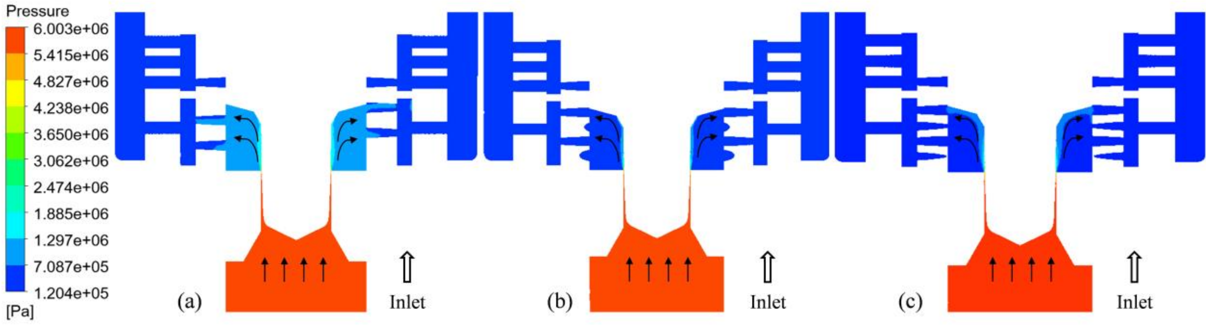

Fig. 11 Control valve pressure cloud diagram. (a) Results before optimization. (b) PPO model optimization results. (c) P-WOA model optimization results

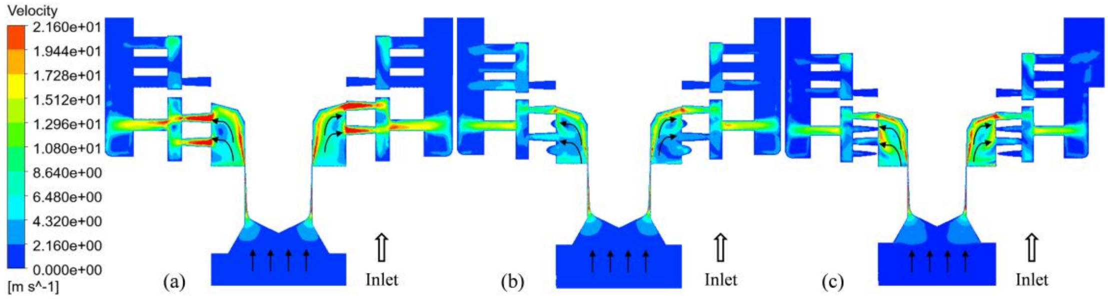

Fig. 12 Control valve velocity cloud diagram. (a) Results before optimization. (b) PPO model optimization results. (c) P-WOA model optimization results

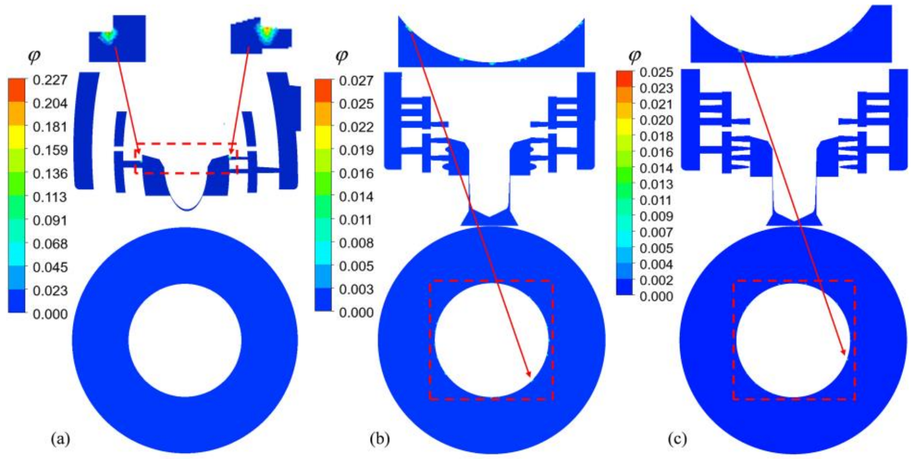

Fig 13 Control valve cavitation area distribution cloud diagram. (a) Results before optimization. (b) PPO model optimization results. (c) P-WOA model optimization results

Figure 12 shows the velocity distribution cloud map before optimization and the two optimization results. There is a low-speed area at the entrance, and the velocity gradient changes little; whereas in the throttling orifice and the flow channel after the hole, the high-speed area is mainly distributed, and the central area of the throttling orifice is particularly significant. The velocity of the fluid medium changes from high speed to low speed from the throttling orifice, and the velocity significantly decrease. This is because when the fluid at the inlet of the control valve flow channel enters the throttling orifice smoothly, the constricting effect of the throttling orifice causes the fluid velocity to increase sharply, change direction, and cause the fluid streamline to contract toward the center of the flow channel. A comparison of Figs 12a, 12b, and 12c, reveals that with a continuous change of the throttling orifice parameters, the velocity distribution in Fig 12a is uneven, which may cause inefficiency and turbulence. However, the flow in Fig 12b is smoother, the turbulence is reduced, and the flow pattern tends to be stable. Figure 12c is the result after optimization using the P-WOA model, showing the most uniform and efficient flow. In this optimized result, the velocity distribution is more uniform in the flow channel and the flow transition is smoother. This optimization further improves fluid dynamics control, reduces turbulence and enhances the overall performance of the system.

Figure 13 shows the cavitation area distribution cloud map of the control valve before optimization and the two optimization results. The results indicate that the cavitation area mainly appears near the flow channel wall behind the throttle hole, and develops in a semicircular arc

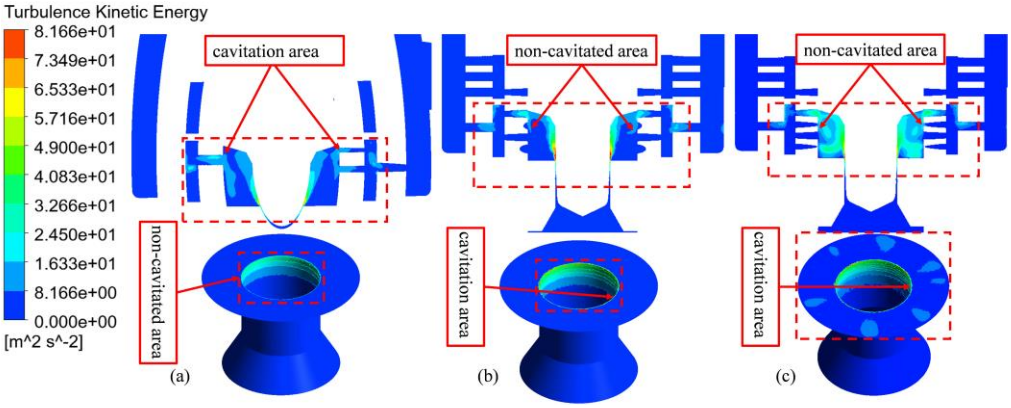

Fig. 14 Control valve turbulent kinetic energy distribution cloud diagram. (a) Results before optimization. (b) PPO model optimization results. (c) P-WOA model optimization results

Table 4 Comparison of the results before and after structural parameter optimization

Physical quantity	Before optimization	PPO	P-WOA	Exp. value
Mass flow (kg/s)	0.644	0.692	0.704	0.747
Gas volume fraction (mm^3)	1.67×10^{-1}	8.39×10^{-4}	3.39×10^{-4}	/

shape toward the center of the flow channel. This phenomenon is attributed mainly to the increase in the flow velocity and the decrease in pressure of the fluid medium at the throttle hole, which leads to the generation of vortices, making the local pressure lower than the saturated vapor pressure, thereby inducing cavitation. Comparing Figes 13a, 13b and 13c, it can be found that the cavitation area in Fig. 13a is concentrated in the throttle hole, with a maximum value of 0.227, indicating that the fluid pressure in the valve changes drastically, which may cause material wear and a reduction in efficiency caused by the cavitation effect. In Figure 13b, the maximum cavitation value is reduced to 0.027, indicating that the optimized valve has achieved remarkable results in reducing cavitation. Figure 13c shows that the cavitation distribution is further optimized, and the maximum cavitation value is reduced to 0.025, which is slightly lower than that of the PPO optimization result. This finding, indicates that the algorithm performs well in further reducing cavitation, almost eliminating the cavitation phenomenon inside the valve, and that the remaining cavitation is distributed mainly near the valve seat wall.

Figure 14 shows the turbulent kinetic energy distribution cloud map before and after the optimization of the control valve and the two optimization results. It can be observed from the figure that in the gas-liquid interface area of the cavitation, the turbulent kinetic energy distribution is obvious and the turbulence intensity is high; while inside the cavitation and in the non-cavitation area, the turbulent kinetic energy is significantly reduced, even to 0, indicating that the turbulence intensity is weak. Comparing Figs 14a, 14b, and 14c, it can be seen that the turbulent kinetic energy distribution before optimization is relatively uneven, while after optimization by the PPO and P-WOA models, the kinetic energy distribution tends to be uniform, especially at the throttling orifice position of the control valve, the kinetic energy is significantly reduced. This shows that after optimization, the turbulent kinetic energy distribution is more uniform, and the TKE near the throttling orifice is significantly reduced, which helps to reduce the cavitation effect caused by high-speed flow, thereby improving the stability and service life of the control valve.

Table 4 shows the comparison results of the three structures with the experimental results. After optimizing the structural parameters of the system by two optimization methods (PPO and P-WOA), the results of the physical quantities have improved. In terms of the mass flow rate and gas volume fraction, the optimization effect of the P-WOA method on the structural parameters of the control valve is better than that of the structure before optimization and the structure after PPO optimization. The experimental value is the actual mass flow rate measured in the laboratory by the structure after P-WOA optimization. Therefore, our proposed method (P-WOA) can effectively optimize the structural parameters of the control valve and reduce the impact of cavitation.

5. Conclusion

The control valve is referred to as the "hands and feet" of the control system. It is one of the many core control elements of fluid devices in the fields of construction, heating systems, petroleum, shipbuilding, chemical industry and marine engineering, and plays a key role in controlling the flow of the system. This study analyzes the cavitation phenomenon in the flow field inside the control valve. By combining theoretical analysis, numerical simulation and experimental research, and introducing reinforcement learning algorithm, the structural parameters of the first-stage sleeve of the control valve are optimized to decrease energy consumption, prevent cavitation and reduce noise. The simulation analysis results show that the high-pressure area is mainly distributed at the inlet, the low-pressure area is located in the downstream flow channel, and the pressure drop is mainly concentrated at the throttling orifice. The cavitation area mainly originates from the throttling orifice and develops in a semicircular shape close to the valve seat wall toward the center of the flow channel. Therefore, optimizing the structural parameters of the control valve is of great significance to reduce the degree of cavitation, reduce the additional flow resistance caused by cavitation, and improve the flow capacity. The proposed method has the following advantages: (1) P-WOA combines the whale optimization algorithm (WOA) and reinforcement learning (RL), which can dynamically adjust parameters and improve the adaptability of the model. (2) By introducing physical constraint penalty terms, the optimization results are ensured to be within a reasonable physical range, thereby enhancing the reliability of the model. Furthermore, the vectorized environment is used to accelerate training, making the model converge faster. By comparing the experimental and numerical results, the structural parameters optimized by the proposed method are in line with engineering practice and can effectively reduce the cavitation phenomenon inside the control valve. Compared with the results of the single PPO algorithm, the effect of P-WOA is better (compared with that before optimization, the gas volume fraction decreases by 99.8%, and compared with the PPO optimization result, the gas volume fraction decreases by 59.6%), and cavitation is effectively suppressed. Since cavitation is the main source of additional energy consumption and noise, the reduction of cavitation means reducing energy loss and reducing flow noise. In addition, the optimized structure significantly decreases the pressure fluctuation of the throttle hole, which helps to reduce the generation of flow-induced noise. These improvements show that the optimization method not only effectively suppresses cavitation, but also plays a positive role in improving energy efficiency and reducing noise.

These research results can be widely applied to safety assurance projects such as multiphase cavitation instability analysis, structural optimization design and local strengthening treatment of control valves or other hydraulic system components, with significant economic and social benefits.

ACKNOWLEDGEMENTS

This work was supported by the National Natural Science Foundation of China (Research Project: 51569012); The Double First-Class Key Program of Gansu Provincial Department of Education; Gansu Province Science and Technology Program Funding: Grant No. 22CX8GA125.

CONFLICT OF INTEREST

The authors declare that they have no known competing financial interests or personal relationships that could have appeared to influence the work reported in this paper.

AUTHORS CONTRIBUTION

Wei Li: Methodology, Writing - Original Draft, Writing – review & editing. **Shuxun Li:** Validation, Supervision, Writing - Review & Editing. **Jianjun Hou:** Investigation, Software, Methodology. **Lingxia Yang:** Investigation, Formal analysis. **Yuhao Tian:** Data curation, Writing – review & editing.

REFERENCES

Akers, M., & Barton, A. (2024). Forming adversarial example attacks against deep neural networks with reinforcement learning. *Computer*, *57*, 88-99. https://ieeexplore.ieee.org/document/10380263

Chen, Z., Yang, S., Li, X., Li, Y., & Li, L. (2023). Investigation on leakage vortex cavitation and corresponding enstrophy characteristics in a liquid nitrogen inducer. *Cryogenics*, *129*, 103606. https://doi.org/10.1016/j.cryogenics.2022.103606

Dadashzadeh, S., Aghaie, M., & Zolfaghari, A. (2022). Optimal design of separation cascades using the whale optimization algorithm. *Annals of Nuclear Energy*, *172*, 109020. https://doi.org/10.1016/j.anucene.2022.109020

Deng, L., Li, W., & Yan, X. (2024). An intelligent hybrid deep learning model for rolling bearing remaining useful life prediction. *Nondestructive Testing and Evaluation*, 1-28. https://doi.org/10.1080/10589759.2024.2385074

Ding, Y., Shen, G., & Wan, W. (2024). Research on a multi-objective optimization method for transient flow oscillation in multi-stage pressurized pump stations. *Water*, *16*(12), 1728. https://doi.org/10.3390/w16121728

Ergur, H. (2022). Multiple performance optimization of a single stage centrifugal pump using an intelligent system approach. *Journal of Applied Fluid Mechanics*, *15*, 1269-1280. https://doi.org/10.47176/jafm.15.04.33040

Fu, Y., Gao, B., Ni, D., Zhang, W., & Fu, Y. (2023). Study on the influence of thermodynamic effects on the characteristics of liquid nitrogen cavitating flow around hydrofoils. *Symmetry*, *15*(10), 1946. https://doi.org/10.3390/sym15101946

Guo, G., Lu, K., Xu, S., Yuan, J., Bai, T., Yang, K., & He, Z. (2023). Effects of in-nozzle liquid fuel vortex cavitation on characteristics of flow and spray: Numerical research. *International Communications in Heat and Mass Transfer*, *148*, 107040. https://doi.org/10.1016/j.icheatmasstransfer.2023.107040

Han, M., Liu, Y., Wu, D., Zhao, X., & Tan, H. (2020). A numerical investigation in characteristics of flow force under cavitation state inside the water hydraulic poppet valves. *International Journal of Heat and Mass Transfer*, *111*, 1-16. https://doi.org/10.1016/j.ijheatmasstransfer.2017.03.100

He, J., Liu, X., Li, B., Qiao, S., & Wang, S. (2023). Visual experiment of hydraulic control valve for distribution characteristics of cavitation flow field. *Research and*

Exploration in Laboratory, *42*, 72-77. https://link.cnki.net/doi/10.19927/j.cnki.syyt.2023.07.015

Homod, R. Z., Mohammed, H. I., & Abderrahmane, A. (2023). Deep clustering of Lagrangian trajectory for multi-task learning to energy saving in intelligent buildings using cooperative multi-agent. *Applied Energy*, *351*, 121843. https://doi.org/10.1016/j.apenergy.2023.121843

Hou, Z., Wang, L., Yan, X., Wang, Z., & An, L. (2021). Study on characteristics of the cavitation bubble dynamics of lithium bromide aqueous solution with ultrasonic interaction. *Journal of Building Engineering*, *44*, 102424. https://doi.org/10.1016/j.jobe.2021.102424

Hu, C., Wang, Q., Gong, W., & Yan, X. (2022). Multi-objective deep reinforcement learning for emergency scheduling in a water distribution network. *Memetic Computing*, *14*, 211-223. https://doi.org/10.1007/s12293-022-00366-9

Jia, X., Zhang, S., & Zhu, Z. (2024). Research on blade tip clearance cavitation and turbulent kinetic energy characteristics of axial flow pump based on the partially-averaged Navier-Stokes model. *Journal of Hydrodynamics*, *36*, 184-201. https://doi.org/10.1007/s42241-024-0014-x

Li, G., Ding, X., Wu, Y., Wang, S., Li, D., Yu, W., Wang, X., Zhu, Y., & Guo, Y. (2022). Liquid-vapor two-phase flow in centrifugal pump: Cavitation, mass transfer, and impeller structure optimization. *Vacuum*, *201*, 111102. https://doi.org/10.1016/j.vacuum.2022.111102

Li, S., Sheng, H., Zhang, W., & Zhao, Y. (2020). Cavitation characteristics and pressure pulsation response of piston type flow control valve. *Journal of Huazhong University of Science and Technology (Natural Science Edition)*, *48*, 44-48+54. https://link.cnki.net/doi/10.13245/j.hust.201208

Li, W., Li, S., Hou, J., Lei, Z., Aierken, T., & Wang, J. (2025). Numerical simulation of control valve flow characteristics based on DE-Bayesian modified turbulence model. *Journal of Building Engineering*, *99*, 111473. https://doi.org/10.1016/j.jobe.2024.111473

Liu, J., Guan, X., & Yang, N. (2023). Bubble-induced turbulence in CFD simulation of bubble columns. Part I: Coupling of SIT and BIT. *Chemical Engineering Science*, *270*, 118528. https://doi.org/10.1016/j.ces.2023.118528

Liu, R., Wang, M., Li, X., Liu, Y., Pei, C., & Gong, J. (2024). Effects of scaling criteria on modelling of multi-phase flow in the packed bed using coarse grain CFD-DEM. *Chemical Engineering Science*, *296*, 120244. https://doi.org/10.1016/j.ces.2024.120244

Mashhadi, A., Sohankar, A., & Moradmand, M.M. (2024). Three-dimensional wake transition of rectangular cylinders and temporal prediction of flow patterns based on a machine learning algorithm. *Physics of Fluids*, *36*, 094138. https://doi.org/10.1063/5.0225180

Mirjalili, S., & Lewis, A. (2016). The whale optimization algorithm. *Advances in Engineering Software*, *95*, 51-67. https://doi.org/10.1016/j.advengsoft.2016.01.008

Mohsenabadi, S. E., Nistor, I., & Mohammadian, A. (2023). CFD modelling of initial stages of dam-break flow. *Canadian Journal of Civil Engineering*, *50*(10), 838-852. https://doi.org/10.1139/cjce-2021-0493

Nadimi-Shahraki, M, H., Zamani, H., Varzaneh, Z., & Mirjalili, S. (2023). A Systematic review of the whale optimization algorithm: theoretical foundation, improvements, and hybridizations. *Archives of Computational Methods in Engineering*, *30*, 4113-4159. https://doi.org/10.1007/s11831-023-09928-7

Naik, D., & Naik, N. (2024). The changing landscape of machine learning: A comparative analysis of centralized machine learning, distributed machine learning and federated machine learning. *Advances in Computational Intelligence Systems*, *1453*, 18-28. https://doi.org/10.1007/978-3-031-47508-5_2

Ou, G., Li, W., Xiao, D., Zheng, Z., Dou, H., & Wang, C. (2015). Numerical investigation on cavitation in pressure relief valve for coal liquefaction. *IOP Conference Series: Materials Science and Engineering*, *72*, 042039. https://iopscience.iop.org/article/10.1088/1757-899X/72/4/042039

Ou, G., Wang, C., & Jin, H. (2024). Erosion characteristics and flashing flow of high-differential-pressure control valves: A numerical study using an erosion-coupled dynamic mesh. *Journal of Applied Fluid Mechanics*, *17*, 559-570. https://doi.org/10.47176/jafm.17.3.2226

Park, S, H., Phan, T, H., Nguyen, V., Duy, T., Nguyen, Q., & Park, W. (2024). Numerical simulation of wall shear stress and boundary layer flow from jetting cavitation bubble on unheated and heated surfaces. *International Journal of Heat and Mass Transfer*, *222*, 125189. https://doi.org/10.1016/j.ijheatmasstransfer.2024.125189

Park, S., Kim, J., Jeong, H, Y., Kim, T., & Yoo, J. (2023). C2RL: Convolutional-contrastive learning for reinforcement learning based on self-pretraining for strong augmentation. *Sensors*, *23*(10), 4946. https://doi.org/10.3390/s23104946

Rabelo, S. N., Paulino, T. F., & Soares, C. P. M. (2023). Mass flow characteristics of CO2 operating in a transcritical cycle flowing through a needle expansion valve in a direct-expansion solar assisted heat pump. *Journal of Building Engineering*, *67*, 105963. https://doi.org/10.1016/j.jobe.2023.105963

Ruetten, E., Leister, N., Karbstein, H, P., & Hakansson, A. (2023). Possibilities and limits of modeling cavitation in high-pressure homogenizers - a validation study. *Chemical Engineering Science*, *283*, 119405. https://doi.org/10.1016/j.ces.2023.119405

Schulman, J., Wolski, F., Dhariwal, P., Radford, A., & Klimov, O. (2017). Proximal policy optimization algorithms. *arXiv:1707.06347*. https://doi.org/10.48550/arXiv.1707.06347

Shijo, J. S., & Behera, N. (2023). Pressure drop prediction in fluidized dense phase pneumatic conveying using machine learning algorithms. *Journal of Applied Fluid Mechanics*, *16*, 1951-1961. https://doi.org/10.47176/jafm.16.10.1869

Trilling, J., Schumacher, A., & Zhou, M. (2024). Reinforcement learning based agents for improving layouts of automotive crash structures. *Applied Intelligence*, *54*, 1751-1769. https://doi.org/10.1007/s10489-024-05276-6

Wadood, A., Khan, B. S., & Albalawi, H. (2024). Design of the novel fractional order hybrid whale optimizer for thermal wind power generation systems with integration of chaos infused wind power. *Fractal and Fractional*, *8*(7), 379. https://doi.org/10.3390/fractalfract8070379

Wang, Q., Wang, J., Zhuang, H., Liu, J., Jiang, B., Song, Y., & Zhang, K. (2024a). Acoustic mechanism and noise reduction optimization of globe valve in air conditioning system. *Journal of Building Engineering*, *89*, 109239. https://doi.org/10.1016/j.jobe.2024.109239

Wang, X., Sun, Q., Wang, T., Ma, J., & Lv, W. (2024b). Study on cavitation noise monitoring and characteristics based on venturi bench test. *Journal of Theoretical and Computational Acoustics, 110819*. https://doi.org/10.1142/S2591728524500099

Wang, X., Wang, Y., Liu H., Xiao, Y., Jiang, L., & Li, M. (2023). A numerical investigation on energy characteristics of centrifugal pump for cavitation flow using entropy production theory. *International Journal of Heat and Mass Transfer*, *201*, 123591. https://doi.org/10.1016/j.ijheatmasstransfer.2022.123591

Xia, Q., Xu, K., Li, M., Hu, K., Song, L., Song, Z., & Sun, N. (2024). Review of attention mechanisms in reinforcement learning. *Journal of Frontiers of Computer Science & Technology*, *18*, 1457-1475. http://fcst.ceaj.org/CN/10.3778/j.issn.1673-9418.2312006

Xie, Y., Yuan, H., Li, T., Chen, E., & Ju, B. (2020). Research on improvement measures of fire protection capacity for UHVDC converter station. *High Voltage Apparatus*, *56*, 241-254. https://doi.org/10.13296/j.1001-1609.hva.2020.01.036

Xin, X., Zhang, Z., Zhou, Y., Liu, Y., Wang, D., & Nan, S. (2024). A comprehensive review of predictive control strategies in heating, ventilation, and air-conditioning (HVAC): Model-free VS model. *Journal of Building Engineering*, *94*, 110013. https://doi.org/10.1016/j.jobe.2024.110013

Yanez, J., & Class, A. G. (2022). Reduced order model of standard k-e turbulence model. *Computers & Fluids*, *245*, 105608. https://doi.org/10.1016/j.compfluid.2022.105608

Yin, Q., Yu, T., Shen, S., Yang, J., Zhao, M., Ni, W., Huang, K., Liang, B., & Wang, L. (2024). Distributed deep reinforcement learning: A survey and a multi-player multi-agent learning toolbox. *Machine Intelligence Research*, *21*, 411-430. https://doi.org/10.1007/s11633-023-1454-4

Zeng, N., Song, D., Li, H., Cheng, Y., & You, Y. (2021). Improved whale optimization algorithm and turbine disk structure optimization. *Journal of Mechanical Engineering*, *57*, 254-265. https://api.semanticscholar.org/CorpusID:245941288

Zhang, G., Wu, X., Wu, Z., Zhang, H., Kim, H., & Lin, Z. (2024). 3-D numerical study of cavitation evolution through a butterfly valve model at different regulating conditions. *Journal of Applied Fluid Mechanics*, *18*, 332-347. https://doi.org/10.47176/iafm.18.2.2629

Zhang, Y., Liu, Y., Liu, S., Gong, Z., & Wu, L. (2023). Transient analysis of a noise suppression method with aerating techniques in capillary tubes. *Thermal Science*, *27*, 4637-4649. https://doi.org/10.2298/TSCI221127093Z

Zhu, Z., Lin, K., Jain, A. K., & Zhou, J. (2023). Transfer learning in deep reinforcement learning: A survey. *IEEE Transactions on Pattern Analysis and Machine Intelligence*, *45*, 13344-13362. https://ieeexplore.ieee.org/document/10172347